Highly doubly excited states of planar helium: Fluctuations in photoionization cross sections

Johannes Eiglsperger
Physik Department, Technische Universität München, 85747 Garching, Germany

Javier Madroñero
Physik Department, Technische Universität München, 85747 Garching, Germany and Laboratoire de Physique Atomique, Moléculaire et Optique (PAMO), Université catholique de Louvain, 1348 Louvain-la-Neuve, Belgium

(Received 23 February 2009; published 21 August 2009; publisher error corrected 21 September 2009)

Photoionization cross sections calculated up to the 20th single ionization threshold of triplet P states of planar helium exhibit fluctuations. These are mainly due to a dominant series of resonances which can be associated with an approximate quantum number $F=N-K$ in accordance with three-dimensional full calculations and experimental observations. As the energy increases the dominant role of a single series as sole contributor is apparently lost as new series start to contribute significantly to the cross sections. This would result in an earlier onset of Ericson fluctuations as in the picture of a single dominant series, where the onset is expected around I_{34}.

DOI: 10.1103/PhysRevA.80.022512 PACS number(s): 32.80.Fb, 05.45.Mt, 32.30.−r, 31.15.A−

I. INTRODUCTION

As first noticed by Poincaré, the classical dynamics of the three-body problem is nonintegrable, which also remains true when gravitational forces are substituted by attractive and repulsive Coulomb forces, such as define the three-body Coulomb problem. Indeed, the electron-electron interaction term in the Hamiltonian of the unperturbed helium atom—which otherwise is just the sum of two hydrogen Hamiltonians with amended nuclear charge—renders the two-electron dynamics in general irregular and chaotic with only small regions of regular motion in the classical phase space [1,2]. Due to the scaling properties of the helium Hamiltonian the regime of highly doubly excited states can be described semiclassically. As a consequence, the quantum spectrum of highly doubly excited states should be influenced by the underlying classical chaotic dynamics and typical signatures of quantum chaos, such as a Wigner distribution of the energy spacings between nearest-neighbor resonances [3] or Ericson fluctuations [4–6], are expected to become observable [7].

Doubly excited states of two-electron atoms are organized in series converging toward the single ionization thresholds (SITs) I_N of $\mathrm{He}(N)^+$ states. Doubly excited states cannot in general be described by a simple model based on independent-particle angular momentum quantum numbers $NLnl$, as was first realized in 1963 through the famous experiment by Madden and Codling [8]. Since then, the regime near the double ionization threshold (DIT) represents a paradigm for electron correlations in atomic systems and has therefore attracted the continuous interest of both theoreticians and experimentalists. A large amount of theoretical and computational effort has been invested in the attempt to improve our understanding of electron correlations in two-electron atoms, see, e.g., [2,9–14] and references therein. For instance, there are certain highly asymmetric and highly correlated states associated to highly correlated classically stable configurations, such as the frozen planet configuration [15]. In addition to the possibility to create nondispersive wave packets [16–18], these frozen planet states raise the question of how their presence affects the Ericson scenario mentioned above, since their autoionization widths become smaller and smaller toward the breakup threshold.

The inherent strongly correlated nature of the doubly excited states requires the introduction of a classification scheme consisting of the approximate quantum numbers (n,N,K,T) [19,20]. Starting from the fourth single ionization threshold members of higher lying series interfere with lower series. Above the eighth ionization series the widths of the resonances can be larger than their separation [11,21]. Whether the overlap of these series and the overlap of the resonances will break down the approximative quantum numbers and will lead to Ericson fluctuations is not clear yet. The understanding of these issues indeed poses a challenge for both experiment and theory. In the recent years an improvement of measurement techniques has allowed a detailed examination of the doubly excited states converging up to the $N=16$ threshold of He [21–23]. From the theoretical side, close to the double ionization threshold the number of open channels increases dramatically. Therefore, currently available full three-dimensional (3D) approaches require rather large basis sets for the representation of the associated eigenvalue problem. Simplified one-dimensional (1D) models or the s^2 model of the three-dimensional atom reduce significantly the calculation difficulties. However, the former models may underestimate the decay rates of the resonances by orders of magnitude [24] and the latter does not resolve all resonances that are important for Ericson fluctuations as observed below. Studies on quantum chaos of the 1D helium atom have predicted Ericson fluctuations in the total photoionization cross sections (TPCS) to be observable above I_{34} [25,26] and studies within the s^2 model find Ericson fluctuations in the partial inelastic cross sections between electrons and He^+ already around I_{16} [27]. On the other hand currently available full 3D approaches are able to describe the spectrum up to the $N=17$ threshold [23]. The analysis of the theoretical and experimental results up to $I_{N=17}$ in [23] reveals a clear dominance of principal Rydberg series in the total photoionization cross section. The hierarchy in the intensities of the resonances reveals that $F=N-K$ is an ap-

proximate quantum number for a large fraction of the states. Consequently Ericson fluctuations are absent in this regime and no transition to full chaos is observed, in clear contradiction with the predictions of simplified models [27].

In this paper, we investigate the TPCS for planar (2D) helium up to the 20th ionization threshold. In contrast to 1D models our approach reproduces correctly the order of magnitude of the widths of doubly excited states [24]. Moreover, our results are in qualitative agreement with full 3D calculations [23]. They show that a large part of the states are associated to the approximate quantum number $F=N-K$. Furthermore, we find that the contribution to the TPCS of the series associated to $F=1$ is dominant; however, the series associated to larger values of F start to compete with the principal series suggesting the onset of Ericson fluctuations in a regime lower than the one predicted by one-dimensional models [23,25].

The paper is organized as follows: in Sec. II we outline our theoretical and numerical setup. This approach is valid for the exact quantum description of field-free planar helium, without adjustable parameters, designed for direct access to the detailed spectral structure of the problem. Section III provides a complete description of the spectral properties of planar helium up to the 20th ionization threshold and discusses the dominance of Rydberg series in the TPCS. Section IV concludes the paper.

II. THEORY AND NUMERICAL IMPLEMENTATION

The computation and analysis of fluctuations in photoionization cross sections of helium demands a description of the helium atom with a minimum of approximations. The electrons are subject to the combined potentials of the nucleus and of the interelectronic interaction which gives rise to a very rich resonance structure close to the total breakup regime.

Therefore, our theoretical approach has to account for the following: (1) the singularities of the Coulomb potentials; (2) the spectrum of the helium atom consisting of bound states and of resonances embedded into the atomic continua; (3) the photon-induced transitions between initial and final states which provide the cross sections; (4) adequate classification schemes of the resonances reflecting the underlying classical chaotic dynamics.

A detailed description of our approach for planar helium has already been presented elsewhere [17,28,29]. We will thus give only a brief review of its most relevant aspects.

A. Hamiltonian

The Hamiltonian of a helium atom with fixed nucleus, neglecting relativistic and QED terms, reads, in atomic units,

$$H=\frac{\vec{p}_1^2+\vec{p}_2^2}{2}-\frac{2}{r_1}-\frac{2}{r_2}+\frac{1}{r_{12}}. \tag{1}$$

Here, r_1 and r_2 are the distances of the electrons from the nucleus and r_{12} is the interelectronic separation.

Both, the classical and the quantum dynamics are governed by Hamiltonian (1). The classical dynamics generated by Hamiltonian (1) is invariant under the scaling transformations [30]

$$H\mapsto |E|^{-1}H,$$

$$\vec{r}_i\mapsto |E|\vec{r}_i,\quad (i=1,2),$$

$$\vec{p}_i\mapsto |E|^{-1/2}\vec{p}_i,\quad (i=1,2), \tag{2}$$

where E is the energy of the two-electron system. The angular momentum thus scales as $L^{sc}=|E|^{1/2}L$. Therefore, for moderate values of L and highly doubly excited states ($E\simeq 0$), the scaled angular momentum is close to zero, tantamount to an almost planar three-body configuration. Precisely this is the semiclassical energy regime where one expects that classical and quantum dynamics are similar. From now on, we confine the dynamics to two dimensions of configuration space, with the Cartesian positions (x_1,y_1) and (x_2,y_2) of the electrons. The planar helium dynamics thus has four degrees of freedom which span an eight-dimensional phase space.

B. Eigenvalue problem

One of the main difficulties to actually perform the diagonalization of Hamiltonian (1) are the Coulomb singularities therein. Nevertheless, by choosing an appropriate representation in parabolic coordinates [28], the singularities are rigorously regularized. The appropriate set of parabolic coordinates is obtained after three subsequent coordinate transformations, which have been treated in detail in [17,28,29]. After multiplication by the Jacobian $B=16r_1r_2r_{12}$ of the transformation the Schrödinger equation of the three-body Coulomb problem takes the form of a generalized eigenvalue problem,

$$A|\Psi\rangle=EB|\Psi\rangle, \tag{3}$$

where $A=BH$ and B are polynomial functions of the coordinates and their derivatives. This leads to a *finite* representation in terms of four sets of creation and annihilation operators, a_j, $a_j^\dagger$, $j=1,2,3,4$. Since each of these pairs of operators can be associated with a harmonic oscillator, this induces a natural basis set composed of tensor products of harmonic oscillator Fock states: $|n_1n_2n_3n_4\rangle=|n_1\rangle\otimes|n_2\rangle\otimes|n_3\rangle\otimes|n_4\rangle$. For example, the total angular momentum L has a simple representation in terms of the number operators $N_j=a_j^\dagger a_j$, $j=1,2,3,4$: $L=(N_1-N_2+N_3-N_4)/4$.

C. Complex dilation

The electron-electron interaction in helium couples different channels of the noninteracting two-electron dynamics and gives rise to resonance states embedded in the continua above the first single electron ionization threshold. To extract the resonance states and their decay rates we use complex rotation (or "dilation") [31–35], which was shown to be applicable for the Coulomb potential in [36].

The complex rotation of any operator by an angle θ is mediated by the nonunitary complex dilation operator

$$R(\theta) = \exp\left(-\theta\frac{\vec{r}\cdot\vec{p}+\vec{p}\cdot\vec{r}}{2}\right), \tag{4}$$

where $\vec{r}$ and $\vec{p}$ represent the four component vector made up of $\vec{r}_1$, $\vec{r}_2$ and $\vec{p}_1$, $\vec{p}_2$, respectively. Rotation of the position and momentum operators in the complex plane according to

$$\vec{r} \to R(\theta)\vec{r}R(-\theta) = \vec{r}\exp(\imath\theta),$$

$$\vec{p} \to R(\theta)\vec{p}R(-\theta) = \vec{p}\exp(\imath\theta), \tag{5}$$

transforms a real representation of Hamiltonian (1) in a complex symmetric operator with complex eigenvalues. However, the spectrum of the rotated Hamiltonian has the following important properties [32,34,36]:

(1) The bound spectrum of H is invariant under the complex rotation.

(2) The continuum states are located on half lines, rotated by an angle -2θ around the ionization thresholds of the unrotated Hamiltonian, into the lower half of the complex plane. In the specific case of the unperturbed 2D helium Hamiltonian (1), in analogy to the 3D case [37], the continuum states are rotated around the single ionization thresholds $I_N=-2/(N-1/2)^2$ a.u. [28], with $N\in\mathbb{N}$.

(3) There are isolated complex eigenvalues $E_{i,\theta}=E_i-\imath\Gamma_i/2$ in the lower half plane corresponding to resonance states. These are stationary under changes in θ provided the dilation angle is large enough to uncover their positions on the Riemannian sheets of the associated resolvent [37,38]. The associated resonance eigenfunctions are square integrable [35] in contrast to the resonance eigenfunctions of the unrotated Hamiltonian. The latter are asymptotically diverging outgoing waves [35,39].

The eigenstates of $H(\theta)=R(\theta)HR(-\theta)$,

$$H(\theta)|\psi_{i,\theta}\rangle = E_{i,\theta}|\psi_{i,\theta}\rangle, \tag{6}$$

are normalized for the scalar product

$$\langle\psi_{j,-\theta}|\psi_{i,\theta}\rangle = \delta_{ij}, \tag{7}$$

and satisfy the closure relation

$$\sum_i |\psi_{i,\theta}\rangle\langle\psi_{i,-\theta}| = 1. \tag{8}$$

Following [40], the Green's function of the rotated Hamiltonian writes

$$G_\theta = \frac{1}{E-H(\theta)} = \sum_i \frac{|\psi_{i,\theta}\rangle\langle\psi_{i,-\theta}|}{E-E_{i,\theta}}, \tag{9}$$

while the relation between the Green's function of the unrotated Hamiltonian and Eq. (9) has been shown [41] to be

$$G(E) = \frac{1}{E-H} = R(-\theta)G_\theta(E)R(\theta). \tag{10}$$

The projection operator on a real energy eigenstate is related to the Green's function through

$$|\phi_E\rangle\langle\phi_E| = \frac{1}{2\imath\pi}[G^-(E)-G^+(E)], \tag{11}$$

with

$$G^\pm(E) = \frac{1}{E\pm\imath\eta-H}, \quad \eta\to 0^+. \tag{12}$$

Using Eqs. (9) and (10) gives for the projection operator on a real energy eigenstate, in terms of the eigenstates of the rotated Hamiltonian,

$$|\phi_E\rangle\langle\phi_E| = \frac{1}{2\imath\pi}\sum_i\left[\frac{R(-\theta)|\psi_{i,\theta}\rangle\langle\psi_{i,-\theta}|R(\theta)}{E_{i,\theta}-E} - \frac{R(\theta)|\psi_{i,-\theta}\rangle\langle\psi_{i,\theta}|R(-\theta)}{E_{i,-\theta}-E}\right]. \tag{13}$$

D. Cross section

Fermi's Golden Rule yields for the photoionization cross section:

$$\sigma(\omega) = \frac{4\pi^2\omega}{c}|\langle\phi_E|T|\phi_E^{\text{in}}\rangle|^2, \tag{14}$$

where $|\phi_E^{\text{in}}\rangle$ denotes the initial state with energy E_{in}, $|\phi_E\rangle$ a state with energy $E=E_{\text{in}}+\omega$, and $T=\vec{e}\cdot\vec{r}$ the dipole operator with the light polarization $\vec{e}$. Combining Eqs. (13) and (14) gives

$$\sigma(\omega) = \frac{2\pi\omega}{\imath c}\sum_i\left[\frac{\langle\phi_E^{\text{in}}|TR(-\theta)|\psi_{i,\theta}\rangle\langle\psi_{i,-\theta}|R(\theta)T|\phi_E^{\text{in}}\rangle}{E_{i,\theta}-E} - \frac{\langle\phi_E^{\text{in}}|TR(\theta)|\psi_{i,-\theta}\rangle\langle\psi_{i,\theta}|R(-\theta)T|\phi_E^{\text{in}}\rangle}{E_{i,-\theta}-E}\right]. \tag{15}$$

Changing θ to $-\theta$ is, for a real representation of the Hamiltonian, equivalent to changing $H(\theta)$ into its complex conjugate, resulting in

$$E_{i,-\theta} = \overline{E_{i,\theta}},$$

$$|\psi_{i,-\theta}\rangle = |\overline{\psi_{i,\theta}}\rangle. \tag{16}$$

As has been stated in [40], Eq. (15) is somewhat formal, as $R(-\theta)|\psi_{i,\theta}\rangle$ is not a well defined state, and $\langle\phi_E^{\text{in}}|TR(-\theta)|\psi_{i,\theta}\rangle$ has to be understood as $\langle\overline{\psi_{i,\theta}}|R(\theta)\overline{T}|\phi_E^{\text{in}}\rangle$. The last expression coincides, for an initial state with a real radial wave function, with $\langle\overline{\psi_{i,\theta}}|R(\theta)T|\phi_E^{\text{in}}\rangle$. The second term of Eq. (15) has to be understood and translated in an analogous manner. Together with Eq. (16) this leads to the final result:

$$\sigma(\omega) = \frac{4\pi\omega}{c}\text{Im}\left[\sum_i\frac{\langle\overline{\psi_{i,\theta}}|R(\theta)T|\phi_E^{\text{in}}\rangle^2}{E_{i,\theta}-E_{\text{in}}-\omega}\right]. \tag{17}$$

Transformation into the appropriate coordinates allows representing the matrix elements of the dipole operator in the creation and annihilation operators, a_j, $a_j^\dagger$, $j=1,2,3,4$.

E. Expectation value of cos θ_{12}

Under complex rotation the expectation value of cos θ_{12} for a given state $|\psi_i\rangle$ of the atom is given by

$$\langle \psi_i | \cos\,\theta_{12} | \psi_i \rangle = \langle \psi_i | \cos\,\theta_{12} R(-\theta) R(\theta) | \psi_i \rangle = \langle \psi_{i,-\theta} | \cos\,\theta_{12} | \psi_{i,\theta} \rangle. \quad (18)$$

Here we have inserted the identity in form of $R(-\theta)R(\theta)$. In addition we have taken into account that $\cos\,\theta_{12}$ and $R(-\theta)$ commute which follows immediately from the definition

$$\cos\,\theta_{12} = -\frac{r_{12}^2 - r_1^2 - r_2^2}{2 r_1 r_2}. \quad (19)$$

After transformation to appropriate parabolic coordinates the matrix elements of $\cos\,\theta_{12}$ can be expressed as polynomials in the coordinates and thus be represented through the creation and annihilation operators, a_j, $a_j^\dagger$, $j=1,2,3,4$.

In practice expression (18) is complex due to numerical rounding errors and due to the truncation of the basis. Nevertheless, for converged resonances its imaginary part is very small. Under this consideration and using Eq. (16), the expectation value of $\cos\,\theta_{12}$ is finally

$$\langle \phi_E | \cos\,\theta_{12} | \phi_E \rangle = \mathrm{Re}(\langle \overline{\psi_{i,\theta}} | \cos\,\theta_{12} | \psi_{i,\theta} \rangle). \quad (20)$$

F. Numerical treatment

Together with the rotation of configuration space by an angle θ, we also introduce a dilation by a positive real number α, such that the (Cartesian) coordinates and momenta transform according to $\vec{r} \to \alpha \vec{r} \exp(\imath\theta)$ and $\vec{p} \to \vec{p} \exp(-\imath\theta)/\alpha$. Since the dilation by a factor α is a unitary transformation described by the unitary operator [39,42]

$$D_\alpha = \exp\left[\imath(\log\,\alpha) \frac{\vec{r}\cdot\vec{p} + \vec{p}\cdot\vec{r}}{2} \right], \quad (21)$$

the spectra of a Hamiltonian H and of the dilated Hamiltonian $H_\alpha = D_\alpha H D_\alpha^\dagger$ are the same. However, when the basis is truncated, the spectrum *does* depend on the parameter α, if the basis set is not large enough. Therefore, α can be used as a variational parameter that has to be optimized.

Due to the polynomial character of the representation in creation and annihilation operators the matrix elements of Eq. (3) have exact analytical expressions. In addition, only a finite number of basis elements $|n_1' n_2' n_3' n_4'\rangle$ are coupled to a given basis element $|n_1 n_2 n_3 n_4\rangle$ which results in a finite number of selection rules. Therefore, combining the rotation by an angle θ with a dilation by a real positive number α [17] and the representation in creation and annihilation operators, the generalized eigenvalue problem (3) can be written as

$$A_\alpha(\theta) | \psi_{i,\theta} \rangle = E_{i,\theta} B | \psi_{i,\theta} \rangle, \quad (22)$$

where $A_\alpha(\theta)$ and B are infinite sparse banded matrices. The basis $|n_1 n_2 n_3 n_4\rangle$ is properly symmetrized and truncated for numerical implementation (for details see [17,29]). Altogether, in our numerical implementation $H_\alpha(\theta)$ and B are represented by sparse banded matrices with typically large dimensions (e.g., $325\,801 \times 16\,293$ for $n_{\mathrm{base}} = \max(n_1,n_2,n_3,n_4) = 395$ for the description of triplet P states around the 20th ionization threshold). The numerical diagonalization of Eq. (22) combines the Lanczos algorithm [43–45] and advanced techniques of parallel programming [46,47] and was carried out on large computers such as the SGI Altix 4700 of the Bayerische Akademie der Wissenschaften [48].

III. RESULTS

As in the three-dimensional case [2], the eigenstates of 2D helium are organized in series converging to single ionization thresholds which all converge to the double ionization threshold at zero energy. The threshold structure of the spectrum is essentially the same as for the case without electron-electron interaction and the location of the various single ionization thresholds is unaffected by the term $1/r_{12}$, since the electron-electron interaction vanishes at large distances. Thus, the Nth threshold energy is given by [28,29]

$$I_N = -\frac{2}{(N-1/2)^2}\ \text{a.u.}, \quad N \in \mathbb{N}, \quad (23)$$

a series which obviously converges to zero with $N \to \infty$. The first series of eigenenergies converges to the threshold $I_1 = -8$ a.u., and above this energy all bound states with $N > 1$ are embedded into the continuum of lower series; i.e., they are resonance states with finite width [37]. Due to the truncation of the basis, the exact thresholds cannot be reached but only effective thresholds I_N^{eff} [46,49]. The spectrum can be classified by the particle exchange symmetry, the symmetry Π_x with respect to the x axis and the absolute value $|l|$ of the angular momentum (or, equivalently, l^2).

In this work we investigate the photoionization cross section for dipole transitions from the lowest lying triplet bound state, with angular momentum $l=0$ and $\Pi_x=+1$, of planar helium. The energy of this state is given by

$$E_{\mathrm{in}} = -8.295\,963\,728\,090\,43\ \text{a.u.}. \quad (24)$$

The dipole operator couples this state with $|l|=1$ triplet states of symmetry $\Pi_x=+1$. The resolution of the TPCS at high energies close to the double ionization threshold requires the accurate calculation of the spectrum associated to these states. A typical spectrum is shown in Fig. 1(a), which has been obtained after the diagonalization of the eigenvalue problem (22) with $\alpha=0.45$ and $\theta=0.25$. Besides the discretized continuum states rotated by 2θ in the complex plane and the resonances there are eigenvalues with positive imaginary part close to I_6 due to the truncation of the basis. In order to exclude these numerical artifacts and nonconverged resonances, all data points have to be checked for convergence with data for other parameter sets. As criterion of convergence for the resonances we used a coincidence, for resonances with different parameter sets $(\alpha, \theta, n_{\mathrm{base}})$, of at least three significant digits for $\mathrm{Re}(E_{i,\theta})$ and two significant digits for $\mathrm{Im}(E_{i,\theta})$. In Fig. 1(a) the converged resonances are highlighted by circles. Figure 1(b) displays all converged resonances with $|\mathrm{Im}(E_{i,\theta})| < 10^{-4}$ a.u. converging to I_N, with $N=4,\ldots,23$. The discretized continuum states depend on the value of θ [see Fig. 1(a)] and to some extent even on the value of α. These are not displayed in Fig. 1(b). As the energy approaches the total breakup threshold the density of states increases dramatically. On the one hand series of states

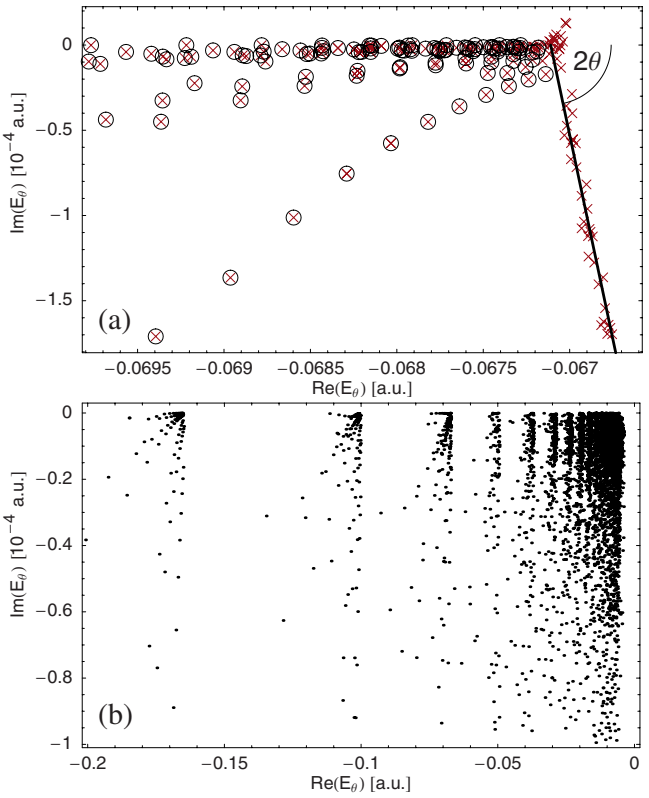

FIG. 1. (Color online) (a) Spectrum of complex rotated triplet helium below the threshold I_6 with parameters α=0.45, θ=0.25, and n_{base}=395. The eigenvalues obtained after numerical diagonalization of Eq. (22) (crosses) contain the converged resonances (circles), the discretized continuum spectrum rotated by an angle 2θ, and some numerical artifacts and nonconverged resonances around the ionization threshold due to the truncation of the basis. (b) Spectrum of resonances of triplet planar helium from below I_4 up to below I_{23}. The data were obtained by several runs of the Lanczos algorithm choosing the shift parameter [29,46] to provide a continuous spectrum. The displayed spectra show the converged resonance eigenenergies extracted from computations with the four parameter sets (θ=0.20, α_c=0.45, and n_{base}=395), (0.20, 0.50, 395), (0.25, 0.45, 395), and (0.25, 0.50, 395). As criterion of convergence a coincidence, of eigenvalues computed for different parameter sets, of at least three (two) significant digits for $\text{Re}(E_{i,\theta})$ ($\text{Im}(E_{i,\theta})$) has been used. Numerical artifacts, discretized continuum states, and nonconverged resonances have been removed.

converging to the different single ionization thresholds will overlap. In 2D helium the fifth Rydberg series overlaps with the sixth series [17] in contrast to 3D helium where the overlapping of series starts with the fourth series. On the other hand, as discussed below, single resonances will overlap with other resonances in the sense that the widths of individual resonances are larger than the separation from their nearest-neighbor resonances. Individual Fano profiles are thus hard or impossible to distinguish and the cross sections exhibit a strongly oscillating or fluctuating pattern around a smooth background. The TPCS can therefore be written as

$$\sigma(\omega) = \sigma_{\text{bg}}(\omega) + \sigma_{\text{fl}}(\omega). \tag{25}$$

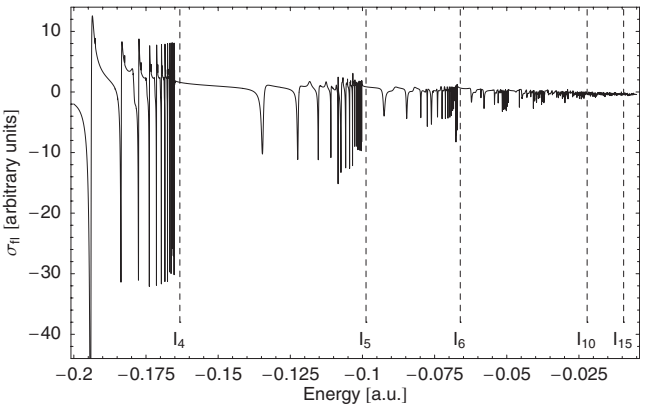

FIG. 2. Calculated fluctuations of the photoionization cross section of triplet planar helium from below I_4 to I_{20}.

The continuum states are responsible for the smooth background $\sigma_{\text{bg}}(\omega)$ of the cross sections and do not affect their fluctuations. Thus, only the resonances contribute to the fluctuating part of the spectrum $\sigma_{\text{fl}}(\omega)$. The numerical calculation of $\sigma_{\text{fl}}(\omega)$ has been accomplished with the help of Eq. (17), where only converged resonances have been taken into account. To guarantee the convergence of our results we have checked the stability of the oscillator strengths $\langle\overline{\psi_{i,\theta}}|R(\theta)T|\phi_E^{\text{in}}\rangle$ and of the fluctuations as function of the parameters θ and α. Converged resonances have been found up to I_{23} and our calculated fluctuations are numerically stable up to I_{20}.

Figure 2 displays $\sigma_{\text{fl}}(E)$. At low energies up to I_7 the cross section is dominated by Fano profiles associated to well-defined isolated resonances. As the energy approaches to the double ionization threshold the cross sections lose their regularity as a consequence of the dramatic increase in the density of states. A second feature of $\sigma_{\text{fl}}(E)$ is also eye-catching: the rather rapid decrease of the fluctuations in magnitude. These two aspects have been subject of intensive investigation in the recent years. On the one hand, a semiclassical scaling law [50] for the fluctuations in the cross section below the double ionization threshold has been derived via closed orbit theory. The scaling law predicts an algebraic decay of the fluctuations,

$$\sigma_{\text{fl}}(E) \propto |E|^{\mu} \quad \text{for} \quad E \to 0^-,$$

$$\mu = \frac{1}{4}\left[\sqrt{\frac{100Z-9}{4Z-1}} + 2\sqrt{\frac{4Z-9}{4Z-1}}\right]. \tag{26}$$

On the other hand, due to the increasing density of states, accompanying an increasing density of fluctuations, near the double ionization threshold there are speculations about the existence of Ericson fluctuations [7,11,23,27,51] in helium [4,5] and their onset.

The scaling law (26) has been corroborated for 1D helium restricted to the *eZe* configuration [50] and experimental evidence has been found below the 17th ionization threshold [52]. An accurate analysis of the fluctuations' scaling law in 2D helium requires going beyond the energy regime we can reach at present. Nevertheless the trend of the behavior pre-

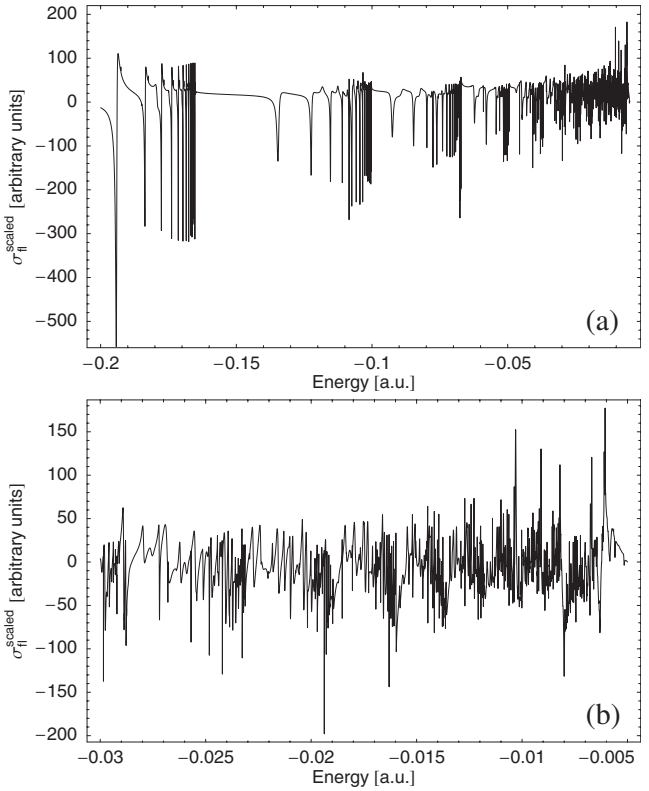

FIG. 3. Scaled fluctuations $\sigma_{\mathrm{fl}}^{\mathrm{scaled}}$ of the cross sections of triplet planar helium. (a) presents $\sigma_{\mathrm{fl}}^{\mathrm{scaled}}$ between I_3 and I_{20}. (b) gives a closeup of the region from below I_9 to below I_{20}. The amplitude of the fluctuations remains approximately constant as function of the energy.

dicted by Eq. (26) can be already recognized in our calculations up to I_{20}: the amplitude of the scaled fluctuations,

$$\sigma_{\mathrm{fl}}^{\mathrm{scaled}}(E) = |E|^{-\mu}\sigma_{\mathrm{fl}}(E), \tag{27}$$

exhibits rather small variations along the energy regime from I_4 to I_{20} as seen in Fig. 3. Since the exponent μ can be written in terms of stability exponents of the triple collision, the total cross sections are expected to be dominated by the low-dimensional collinear *eZe* dynamics. This interpretation is consistent with the observations by Jiang *et al.* [23]: only very few resonances contribute significantly to the photoionization cross section in the region from I_9 to I_{16} and the series of contributing resonances are associated with (small) constant values of $F=N-K$, where N and K are approximate quantum numbers from Herrick's algebraic classification [19,20]. In addition, the *eZe* configuration can indeed be identified with the maximum value of $K=N-1$, i.e., $F=N-K=1$. More precisely, the number K is related to the expectation value of cos θ_{12}, where θ_{12} is the angle between the two electron position vectors $\vec{r}_1$ and $\vec{r}_2$, through the relation

$$\langle \cos\,\theta_{12}\rangle \overset{n\to\infty}{\to} -\frac{K}{N}. \tag{28}$$

Therefore, K approaches $K_{\max}=N-1$ when cos θ_{12} is close to -1.

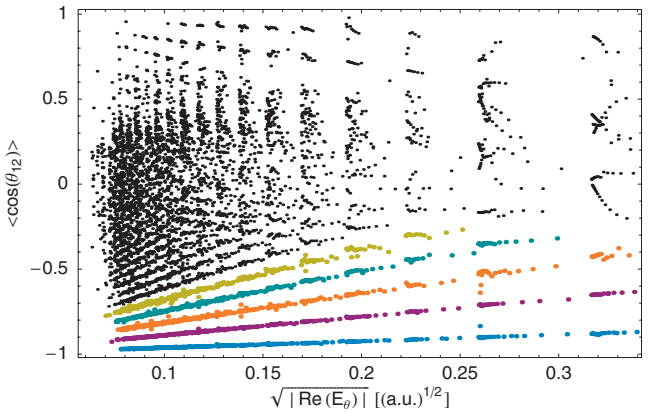

FIG. 4. (Color) Calculated $\langle \cos\,\theta_{12}\rangle$ values as a function of resonance energy E below the 20th threshold. The region $|\langle \cos\,\theta_{12}\rangle| < 0.5$ also includes some converged resonances up to below I_{23}. Each point represents a particular triplet state resonance with $\Pi_x=+1$ and $|l|=1$. The resonances are displayed in color according to their allocation to Rydberg series: • (first), • (second), • (third), • (fourth), • (fifth), and • for resonances not identified with any one of these series.

The algebraic classification can be applied to the 2D model of helium by setting the value $T=0$ [24]. Thus, the expectation value of cos θ_{12} provides information about the approximative quantum number F also in the planar case. Figure 4 presents a plot of the calculated expectation values of $\langle \cos\,\theta_{12}\rangle$ as a function of $\sqrt{|\mathrm{Re}(E_\theta)|}$ for all converged resonances below I_4 up to I_{23}. A clear decomposition into series of resonances can be identified for $\langle\cos(\theta_{12})\rangle \lesssim -0.5$. The values of $\langle\cos(\theta_{12})\rangle$ in such series decrease smoothly with decreasing values of $\sqrt{|\mathrm{Re}(E_\theta)|}$. This may be ascribed to the influences of perturbers with different K values that belong to Rydberg series below the next higher thresholds, i.e., a strong mixing of resonances with different N and K, but the same $N-K$. The approximate quantum number $F=N-K$ thus allows the classification of these series of resonances, of which all members lie on straight lines. The data presented in Fig. 4 illustrate that the number of these series increases with decreasing distance to the double ionization threshold and no mixing of resonance subsets with different F is found for $\langle\cos(\theta_{12})\rangle < -0.5$. In addition the straight lines for series classified by a constant value of F would cross each other at a value of $\langle\cos(\theta_{12})\rangle=-1$ at the double ionization threshold. In this limit these resonances correspond to the *eZe* configuration, which is stable under angular perturbations, but unstable under radial perturbations. Therefore, the existence of the approximative quantum number F can be understood by the regularity in the angular direction in helium, though the radial motion remains chaotic.

In Fig. 4 it is also possible to identify different series of resonances in the region where $\langle\cos(\theta_{12})\rangle$ is close to +1. The value of $\langle\cos(\theta_{12})\rangle$ for each of such series increases systematically, however, its behavior is not smooth. The lowest states of a Rydberg series are apparently always above the next lowest single ionization threshold. Therefore, no mixing between N and K takes place. Resonances in this region can be associated with the *Zee* configuration (also called the frozen planet configuration). The stability of this configuration

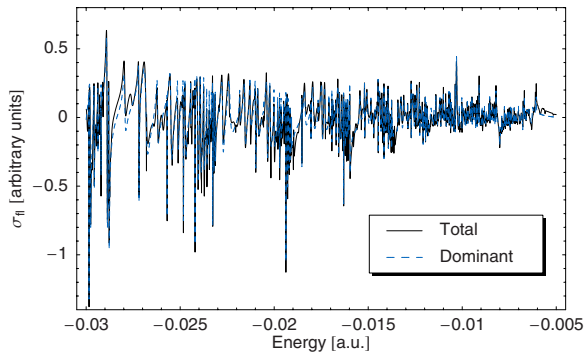

FIG. 5. (Color online) Comparison of the fluctuations of the photoionization cross sections from I_9 up to I_{20} including all resonances (solid line) and resonances with $F=1$ only (dashed line).

in both the radial and the angular directions explains why also N and K remain approximate quantum numbers.

The region $|\langle\cos(\theta_{12})\rangle|<0.5$ is characterized by strong mixing between the numbers N, K, and F, in agreement with the instability of the classical motion of the associated configurations. Thus, the electron motion in this region is highly uncorrelated, which is also reflected in the convergence of our results: resonances above I_{20} are convergent almost exclusively if $|\langle\cos(\theta_{12})\rangle|<0.5$.

The approximate classification of helium resonances unveiled in Fig. 4 allows us to study separately the contributions of different series to the photoionization cross sections. Indeed, only a small fraction of states contribute significantly to the cross section. For triplet states the resonances which yield major contributions are characterized by odd values of F,

$$F = 2m + 1, \quad m \in \mathbb{N}_0, \tag{29}$$

while series with even F and all resonances that cannot be characterized by F—e.g., those resonances close to the DIT for which $-0.5 \lesssim \langle\cos\theta_{12}\rangle \lesssim 0.5$—result in almost no contribution. This is a consequence of the nodal structure of the initial and final wave functions which leads to the propensity rules for dipole transitions [12,53,54]. In the case of singlet states the main contributors correspond to even values of F [23].

The data available at present demonstrate that the size of the contributions decreases with increasing value of m in Eq. (29) resulting in a dominant series with $F=1$. In Fig. 5, a comparison of the fluctuations of the photoionization cross section of the dominant resonance series and the one including all resonances is presented. The comparison illustrates that the subset of resonances with $F=1$ resembles the cross section quite well and therefore that this group of resonances truly yields the dominant contributions.

The picture described above seems also to be reflected in the structure of the contributing series in the complex plane. Figure 6 depicts the imaginary part of the resonances of the first up to the fourth Rydberg series identified in Fig. 4 as a function of $N(E)=\sqrt{-2/E}+1/2$, with $E=\mathrm{Re}(E_\theta)$. Odd series [Figs. 4(a) and 4(c)] are distributed almost homogeneously even at low energies, while the noncontributing even series exhibit a regular distribution at rather high energies. In Figs. 4(b) and 4(d) it is possible to recognize the Rydberg series converging to the single ionization thresholds I_N up to $N\approx 12$, which indicates the absence of intruders from other series.

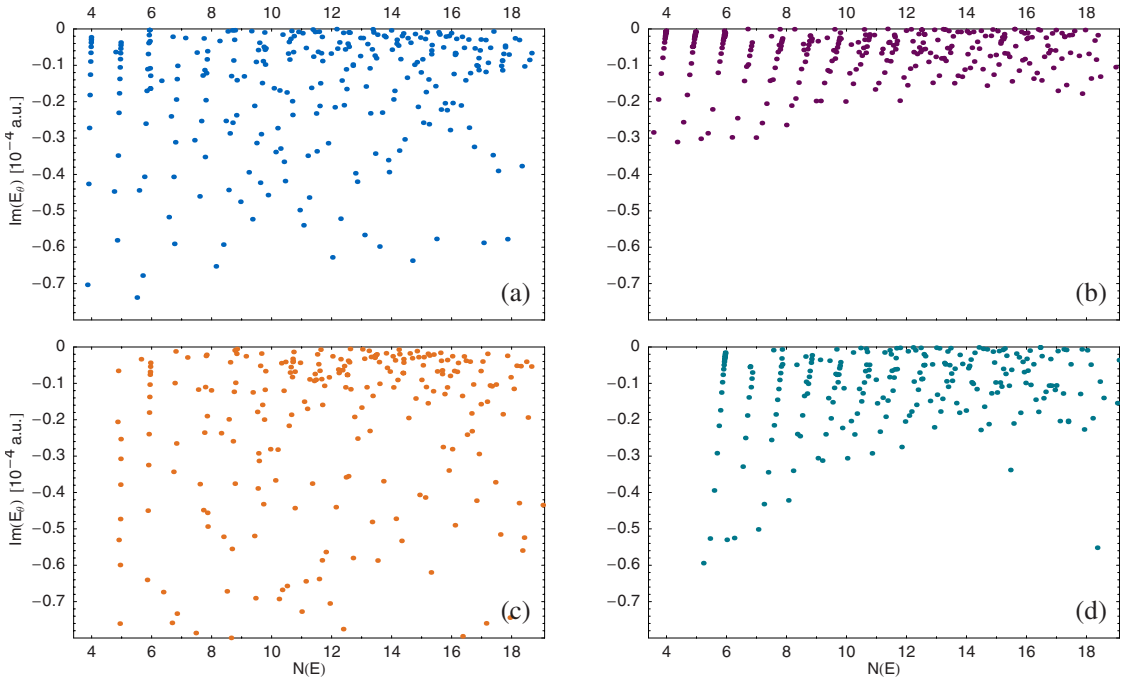

FIG. 6. (Color online) Resonances of triplet planar helium from I_3 up to I_{23} belonging to the series labeled by $F=1$ (a), $F=2$ (b), $F=3$ (c), and $F=4$ (d) identified in Fig. 4. To illustrate the underlying structure the half width of the resonances is shown as a function of $N(E)=\sqrt{-2/E}+1/2$, with $E=\mathrm{Re}(E_\theta)$. Integer values of $N(E)$ denote the single ionization thresholds. The series associated to the odd values of F exhibit a disorder structure already at low energies in contrast to the even series.

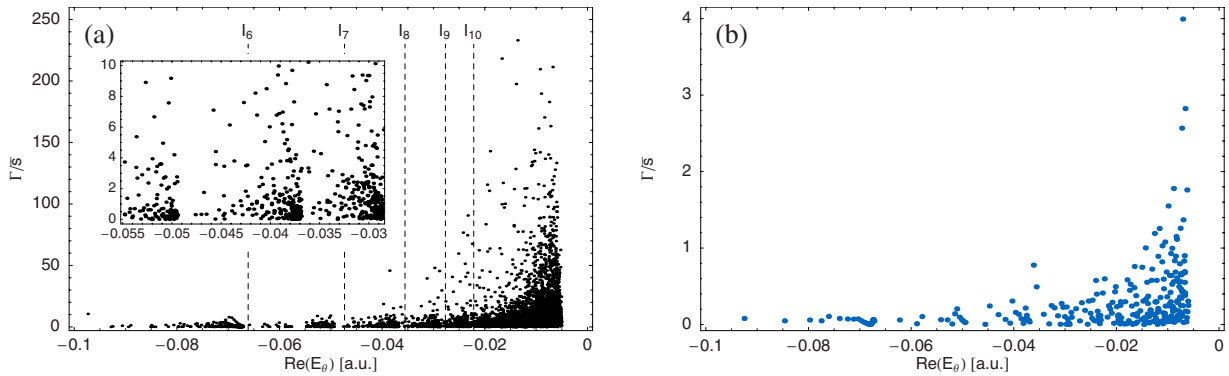

FIG. 7. (Color online) Widths in units of the mean level spacing $\bar{s}$. (a) shows the widths of all resonance states found in this energy regime, with the inset giving a closeup of the regime around I_7 to I_9, while (b) includes exclusively resonances characterized by $F=1$. The way $\bar{s}$ is determined is described in the Appendix with $\gamma=0.1$, $m=30\,000$, and $\xi=1$.

The existence of a dominant subset of resonances has important consequences for the discussion of Ericson fluctuations in the cross sections. We will demonstrate this in a rather crude way by computing a kind of local mean level spacing $\bar{s}$ for converged resonances (see the Appendix) and comparing this to the resonance widths. In Fig. 7 the resonance widths in units of the computed local mean level spacing are displayed. Figure 7(a) clearly illustrates that if one considers all resonances the condition $\bar{\Gamma} \gg \bar{s}$ is already met around I_9 and therefore the Ericson regime is reached. At energies as high as I_{20} more than 90% of the resonances overlap. From this one might expect that single peaks in the cross sections observed in Fig. 3 have random character and are not the result of individual resonances. However, Fig. 7(b) indicates that the resonances of the dominant series have not reached the Ericson regime yet, since the condition $\Gamma_i \geq \bar{s}$ is only fulfilled by a small fraction of resonances and therefore $\bar{\Gamma} \gg \bar{s}$ is not satisfied. The expected value of $\cos\,\theta_{12}$ for the resonances belonging to the $F=1$ series is close to -1 even at low energies and approaches -1 rather fast as the energy increases. Therefore, practically all of these resonances can be associated to the collinear *eZe* configuration. Provided the picture of a dominant series remains valid for high enough energies, Ericson fluctuations in helium are expected around I_{34}.

On the one hand, neither currently available studies of the full 3D problem nor experimental observations [23] supply any evidence for the mixture of series with different approximative quantum numbers F or for the loss or existence of the dominant role of a single series above I_{17}. On the other hand, the decay behavior of fluctuations from different series is not known at low energies, though it is expected to decay according to Eq. (27) at the breakup threshold. Therefore, it is not entirely clear whether the picture described above holds for the whole energy region up to the double ionization threshold. In particular the influence of other series characterized by F has to be understood. In order to investigate this issue we have studied the contributions to the photoionization cross section of the first five series of resonances separately. In Fig. 8 the contributions of the series with $F=1$, $F=3$, and $F=5$ and the contribution of the remaining resonances are presented. A direct comparison of the plots in Fig. 8 provides a rough estimate of the amplitudes of the fluctuations. The typical magnitude of the fluctuations for the resonance series $F=1$ around I_9 is about three times larger than the one for the $F=3$ series and about ten times larger than the one for the $F=5$ series. Nevertheless, we observe that the decay of the magnitude of the fluctuations is more rapid for series with smaller F; e.g., around I_{18} the rate for the typical magnitude of the fluctuations for the series $F=1$ to the one for the series $F=3$ decreased from three to slightly less than two and the one between $F=1$ and $F=5$ from ten to around five. This might eventually lead to a breakdown of the dominant series picture. Instead one might have to consider more and more resonance series with odd F the closer one gets to the double ionization threshold, where the fluctuations of each of these series are comparable in magnitude and which lead to an earlier onset of Ericson fluctuations than expected for the 1D helium picture. The slower decay of the fluctua-

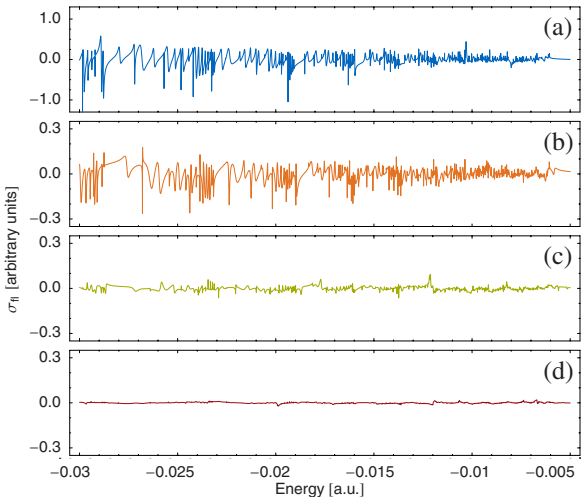

FIG. 8. (Color online) Contributions of subsets of resonances to the fluctuations of the photoionization cross section from below I_9 to below I_{20}. The fluctuations due to the series $F=1$, $F=3$, and $F=5$ are shown in (a), (b), and (c), respectively. The contributions from all remaining resonances are depicted in (d). The rapid decrease in the amplitudes in (a) in comparison to (b) suggests a competition between the $F=1$ and $F=3$ series and an eventual loss of the dominant role of the $F=1$ series.

tions for larger vales of F might be due to the fact that these states are still farther from being collinear than the ones with $F=1$ at low energies, though at the total fragmentation threshold all those series apparently converge to the collinear configuration.

IV. SUMMARY AND CONCLUSIONS

We have presented the computed fluctuating part of the TPCS of doubly excited triplet P states in planar helium up to the ionization threshold I_{20}. The fluctuations of the TPCS follow the behavior predicted by the scaling law given in [50]. $F=N-K$ is found to be an approximate quantum number of states as in the full 3D atom [23]. This imposes a hierarchy on the contributions to the TPCS, where the subset of resonances with $F=1$ gives the dominant contribution. The regime of overlapping resonances is already reached around ionization threshold I_9; however, the resonances of the dominant series do—at least up to I_{20}—not fulfill the overlap criterion $\bar{\Gamma} \gg \bar{s}$. Therefore, Ericson fluctuations are absent in the TPCS. Nevertheless, with decreasing distance to the double ionization threshold the dominance of the $F=1$ series of resonances apparently breaks down as more and more other subsets of resonances start to contribute significantly to the TPCS. This would lead to an earlier onset of Ericson fluctuations than expected in the picture of a single dominant series.

ACKNOWLEDGMENTS

It is a pleasure to thank Dominique Delande and Nark Nyul Choi for lots of illuminating discussions and insight, and we are indebted to Harald Friedrich and Patrick Raab for enlightening discussions and for carefully reading this paper. Access to the computing facilities of the Leibniz-Rechenzentrum der Bayerischen Akademie der Wissenschaft as well as financial support by Deutsche Forschungsgemeinschaft under Contract No. FR 591/16-1 is gratefully acknowledged. J.M. gratefully acknowledges support by the FNRS ("Bourse postdoctorale FNRS dans le cadre de la convention IISN No. 4.4503.02").

APPENDIX: COMPUTATION OF $\bar{s}$

The concern of this appendix is the method for the computation of a local mean level spacing $\bar{s}$ at energies within the energy interval $[E_{\min}, E_{\max}]$ $(E_{\max}<0)$. The main difficulty to achieve this purpose is the inhomogeneous distribution of the resonances, of which the density increases drastically close to the SIT. For the computation of $\bar{s}$, m equally spaced points E_ν, $\nu=1,\ldots,m$, are chosen within the interval $[E_{\min}, E_{\max}]$. Around each E_ν the resonances in the interval $I_\nu=[E_\nu-\frac{\gamma}{\xi+1}x, E_\nu+\frac{\xi\gamma}{\xi+1}x]$ are considered. Here $x=E_{\max}-E_\nu$, γ defines the relative length of the interval I_ν compared to x, and ξ is the proportion of the interval I_ν which is situated above E_ν to the one below E_ν (see Fig. 9). For a given value of $\gamma<1$ the length of intervals I_ν decreases as the E_ν gets closer to $E_{\max}$. Though we do not have control on the number of resonances $N_{\text{res}}^{(\nu)}$ within the intervals I_ν, in this way we

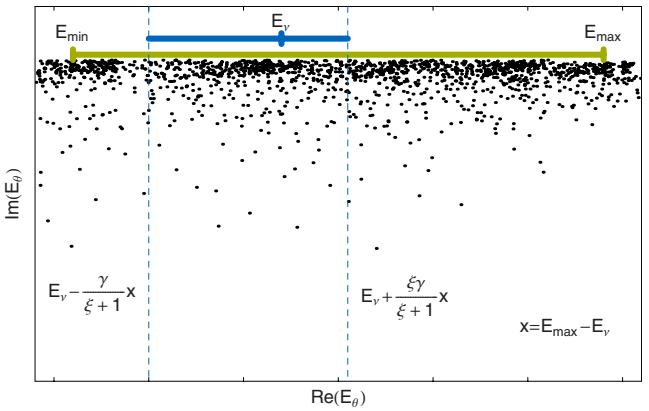

FIG. 9. (Color online) Schematic illustration of the determination of $\bar{s}$.

guarantee that the variations on $N_{\text{res}}^{(\nu)}$ for different values of ν are not as dramatic as for the case when all intervals have the same length. Similarly the parameter ξ is used to tune the ratio of the number of resonances above E_ν within I_ν to the number of resonances below. The local mean level spacing is computed via

$$\bar{s}_\nu = \frac{\gamma(E_{\max}-E_\nu)}{N_{\text{res}}^{(\nu)}}. \tag{A1}$$

Now we calculate an estimate for ξ for which the number of states contained in the lower part of the interval is equal to the one of the upper part. For this we consider a single Rydberg series below a determined threshold. For this crude estimate we assume that we have only one active electron. Starting from an interval $[E_{n-\Delta n}, E_{n+\Delta n}]$ around the state E_n, which includes Δn states above and below the state E_n, the absolute values of energy differences between E_n and the upper and lower boundary of the interval are given by

$$\begin{aligned}\Delta E_+ &= E_{n+\Delta n} - E_n \\ &= -\frac{1}{2\left(n+\Delta n-\frac{1}{2}\right)^2} + \frac{1}{2\left(n-\frac{1}{2}\right)^2} \\ &= \frac{\Delta n(2n+\Delta n-1)}{2\left(n-\frac{1}{2}\right)^2\left(n+\Delta n-\frac{1}{2}\right)^2},\end{aligned}$$

$$\Delta E_- = E_n - E_{n-\Delta n} = \frac{\Delta n(2n-\Delta n-1)}{2\left(n-\frac{1}{2}\right)^2\left(n-\Delta n-\frac{1}{2}\right)^2}, \tag{A2}$$

where n is the excitation of the state with energy E_n. Since we are interested in the behavior immediately below single ionization thresholds, this leads to the assumption $n \gg \Delta n$, under which the proportion $\xi=\Delta E_+/\Delta E_-$ gives

$$\xi = \frac{(2n+\Delta n-1)\left(n-\Delta n-\frac{1}{2}\right)^2}{(2n-\Delta n-1)\left(n+\Delta n-\frac{1}{2}\right)^2} \overset{n\gg\Delta n}{\longrightarrow} 1. \qquad \text{(A3)}$$

A comparison of computations of $\bar{s}$ with varying ξ and γ ($\xi \in [\frac{1}{3}, 1]$, $\gamma \in [0.05, 0.2]$) shows that there is almost no dependence of $\bar{s}$ on these parameters.

[1] K. Richter, G. Tanner, and D. Wintgen, Phys. Rev. A **48**, 4182 (1993).
[2] G. Tanner, K. Richter, and J.-M. Rost, Rev. Mod. Phys. **72**, 497 (2000).
[3] O. Bohigas, M. J. Giannoni, and C. Schmit, Phys. Rev. Lett. **52**, 1 (1984).
[4] T. Ericson, Phys. Rev. Lett. **5**, 430 (1960).
[5] T. Ericson, Ann. Phys. **23**, 390 (1963).
[6] J. Madroñero and A. Buchleitner, Phys. Rev. Lett. **95**, 263601 (2005).
[7] R. Blümel, Phys. Rev. A **54**, 5420 (1996).
[8] R. P. Madden and K. Codling, Phys. Rev. Lett. **10**, 516 (1963).
[9] C. D. Lin, Phys. Rep. **257**, 1 (1995).
[10] A. Bürgers, D. Wintgen, and J.-M. Rost, J. Phys. B **28**, 3163 (1995).
[11] B. Grémaud and D. Delande, Europhys. Lett. **40**, 363 (1997).
[12] J. M. Rost, K. Schulz, M. Domke, and G. Kaindl, J. Phys. B **30**, 4663 (1997).
[13] E. Foumouo, G. L. Kamta, G. Edah, and B. Piraux, Phys. Rev. A **74**, 063409 (2006).
[14] J. Eiglsperger, B. Piraux, and J. Madroñero, preceding paper, Phys. Rev. A **80**, 022511 (2009).
[15] K. Richter and D. Wintgen, Phys. Rev. Lett. **65**, 1965 (1990).
[16] P. Schlagheck and A. Buchleitner, Eur. Phys. J. D **22**, 401 (2003).
[17] J. Madroñero and A. Buchleitner, Phys. Rev. A **77**, 053402 (2008).
[18] J. Madroñero, A. Ponomarev, A. R. R. Carvalho, S. Wimberger, C. Viviescas, A. Kolovsky, K. Hornberger, P. Schlagheck, A. Krug, and A. Buchleitner, Adv. At., Mol., Opt. Phys. **53**, 33 (2006).
[19] O. Sinanoğlu and D. R. Herrick, J. Chem. Phys. **62**, 886 (1975).
[20] D. R. Herrick and O. Sinanoğlu, Phys. Rev. A **11**, 97 (1975).
[21] A. Czasch *et al.*, Phys. Rev. Lett. **95**, 243003 (2005).
[22] M. Domke, K. Schulz, G. Remmers, G. Kaindl, and D. Wintgen, Phys. Rev. A **53**, 1424 (1996).
[23] Y. H. Jiang, R. Püttner, D. Delande, M. Martins, and G. Kaindl, Phys. Rev. A **78**, 021401 (2008).
[24] J. Madroñero, P. Schlagheck, L. Hilico, B. Grémaud, D. Delande, and A. Buchleitner, Europhys. Lett. **70**, 183 (2005).
[25] R. Blümel and W. P. Reinhardt, *Chaos in Atomic Physics* (Cambridge University Press, Cambridge, 1997).
[26] R. Püttner, B. Grémaud, D. Delande, M. Domke, M. Martins, A. S. Schlachter, and G. Kaindl, Phys. Rev. Lett. **86**, 3747 (2001).
[27] J. Xu, A.-T. Le, T. Morishita, and C. D. Lin, Phys. Rev. A **78**, 012701 (2008).
[28] L. Hilico, B. Grémaud, T. Jonckheere, N. Billy, and D. Delande, Phys. Rev. A **66**, 022101 (2002).
[29] G. J. Madroñero Pabón, Dissertation, Ludwig-Maximilians-Universität München, 2004 (http://edoc.ub.uni-muenchen.de/archive/00002187).
[30] I. C. Percival, Proc. R. Soc. London, Ser. A **353**, 289 (1977).
[31] J. Aguilar and J. M. Combes, Commun. Math. Phys. **22**, 269 (1971).
[32] E. Balslev and J. M. Combes, Commun. Math. Phys. **22**, 280 (1971).
[33] B. Simon, Ann. Math. **97**, 247 (1973).
[34] W. P. Reinhardt, Annu. Rev. Phys. Chem. **33**, 223 (1982).
[35] Y. Ho, Phys. Rep. **99**, 1 (1983).
[36] S. Graffi, V. Grecchi, and H. J. Silverstone, Ann. Inst. Henri Poincaré **42**, 215 (1985).
[37] M. Reed and B. Simon, *Methods of Modern Mathematical Physics* (Academic, New York, 1978), Vol. IV.
[38] M. Pont and R. Shakeshaft, Phys. Rev. A **43**, 3764 (1991).
[39] L. D. Landau and E. M. Lifschitz, *Lehrbuch der Theoretischen Physik: III. Quantenmechanik* (Akademie-Verlag, Berlin, 1979).
[40] A. Buchleitner, B. Grémaud, and D. Delande, J. Phys. B **27**, 2663 (1994).
[41] B. R. Johnson and W. P. Reinhardt, Phys. Rev. A **28**, 1930 (1983).
[42] D. Delande, Thèse d'état, Université Pierre et Marie Curie (Paris 6), 1988.
[43] C. Lanczos, J. Res. Natl. Bur. Stand. **45**, 255 (1950).
[44] B. N. Parlett and D. S. Scott, Math. Comput. **33**, 217 (1979).
[45] T. Ericsson and A. Ruhe, Math. Comput. **35**, 1251 (1980).
[46] A. Krug, Dissertation, Ludwig-Maximilians-Universität München, 2001 (http://edoc.ub.uni-muenchen.de/archive/00000336).
[47] http://www.mpi-forum.org/docs/docs.html
[48] http://www.lrz-muenchen.de/services/compute/linux-cluster/
[49] A. Buchleitner, D. Delande, and J.-C. Gay, J. Opt. Soc. Am. B **12**, 505 (1995).
[50] C. W. Byun, N. N. Choi, M.-H. Lee, and G. Tanner, Phys. Rev. Lett. **98**, 113001 (2007).
[51] R. Blümel and U. Smilansky, Phys. Rev. Lett. **60**, 477 (1988).
[52] G. Tanner, N. N. Choi, M.-H. Lee, A. Czasch, and R. Dorner, J. Phys. B **40**, F157 (2007).
[53] J. M. Rost and J. S. Briggs, J. Phys. B **23**, L339 (1990).
[54] K. Richter, J. S. Briggs, D. Wintgen, and E. A. Solov'ev, J. Phys. B **25**, 3929 (1992).